Supplemental Material for:

Deformation conditions during syn-convergent extension along the Cordillera Blanca shear zone (CBSZ), Peru

Cameron A. Hughes[1], Micah J. Jessup[1], Colin A. Shaw[2], Dennis L. Newell[3]

[1]Department of Earth and Planetary Sciences, University of Tennessee- Knoxville, 1412 Circle Drive, Knoxville, TN, USA, 57996-1410
[2]Department of Earth Sciences, Montana State University, P.O. Box 173480, Bozeman, MT, USA, 59717-3480
[3]Department of Geology, Utah State University 4505 Old Main Hill, Logan, UT, USA, 84322

Contents of this file

TEXT S1.

Titanium in quartz produces a detectable cathodoluminescence (CL) signal, which can aid in evaluating possible mineral zonation or multiple generations of quartz growth. Quartz luminescence over a broad spectrum can be due to a range of impurities, such as lattice defects or incorporation of trace elements. Titanium luminesces at 330-340 nm wavelengths and up to 400 nm wavelengths (blue-violet), with greater amounts of Ti producing a stronger signal. Filtering CL images to specific wavelengths can allow for evaluation of Ti zoning or overgrowths (Spear and Wark, 2009; Gotze et al., 2012). This is important in distinguishing between multiple potential generations of quartz, as even minor variations in Ti concentration must be evaluated texturally to determine which concentrations are representative of different deformation time stamps. CL images were captured using the CITL CL8200 Mk5-2 Optical Cathodoluminescence System, mounted on a Nikon Eclipse E400 microscope and attached to an Optronics camera, at University of Tennessee-Knoxville. Operating conditions were 256 µA current and 20 kV electron beam. Images were filtered for blue wavelength through manually variable exposures, where blue exposures were set to between 6 minutes, 49 seconds and 21 minutes, 59 seconds. Images were captured under Turbo mode via Magnafire software and CCD camera such that locations imaged with CL were not exposed for longer than ~8 minutes, thus minimizing effects of shifting emission spectra with time (Götze, 2002).

Spot analyses for Titanium-in-Quartz (TitaniQ) thermometry were conducted using the EMPA at UTK. Two to three spectrometers (PET, LLIF, LLIF or PET, LLIF) were used to count Ti Kα X-rays. Peak count times were 960 s (alternating between 192 s on peak, 96 s on high and low backgrounds), yielding a detection limit of 11 ppm. Accuracy of measurements was evaluated against synthetic quartz crystals containing known Ti concentrations and against Herkimer quartz as a blank.

TEXT S2.

Raw data was processed in Channel 5 to remove wild spikes (individual pixels with orientations dissimilar to all 8 surrounding neighbors), to adjust misindexed pixel orientations to 5 nearest neighbors, and to remove systematic misindexing of grains at orientations 60° (±5°) to the {0001} (or c) axis to account for quartz pseudosymmetry. Subsequent data processing, pole figure construction, and calculations of fabric strength were completed using the MTEX toolbox for MATLAB (Hielscher and Schaeben, 2008; Mainprice et al., 2015).

Grain size is calculated as the diameter of an equivalent-area circular grain. The root mean square of grain size distributions generated from Channel 5 HKL Tango software is used in paleopiezometry calculations. Grains outside of the 95% threshold of grain size distributions were checked against grain size maps to evaluate if they were

relict (outlier of largest grains) or false grains (outlier of smallest grains) and removed from the final distribution used for paleopiezometry.

TEXT S3.

Geochemical modeling may help to resolve the uncertainty in a_{TiO_2} in the system and application of instrumentation with significantly lower (i.e. ppb) detection limits, such as laser ablation-inductively coupled plasma- mass spectrometry (< 1 ppm detection limit, Haertel et al., 2013; Huang and Audétat, 2012) or secondary ion mass spectrometry (<100 ppb detection limit, (Cross et al., 2015; Xia and Platt, 2018) could aid in refining temperature estimates. However, these techniques are outside the scope of this paper.

Discussion of TitaniQ reliability in the CBSZ

TitaniQ and ASIM deformation temperatures are in agreement within error, assuming α_{TiO_2} of 0.5-0.8 using the Thomas et al (2010) calibration. Limitations to the applications of TitaniQ to CBSZ rocks are discussed below, including thermometer calibration, activity constraints, and instrumental precision. The Huang and Audétat (2012) calibration is derived from a quartz bar grown synthetically by dissolution and reprecipitation. This calibration is dependent on growth rate, having only been calibrated for Ti concentrations in the slowest grown quartz samples (Huang and Audétat, 2012; Nachlas and Hirth, 2015). Huang and Audétat (2012) tested their calibration against igneous quartz with independently estimated temperatures where Ti activities were between 0.15 and 0.6, and found their TitaniQ calibration to be in agreement with independent temperature estimates. Later experimental studies found Ti concentrations to be independent of growth rate, calling the applicability of the Huang and Audétat (2012) calibration into question and confirming the original Thomas et. al. (2010) calibration (Nachlas and Hirth, 2015; Thomas et al., 2015).

Ti concentrations for analyzed samples from the CBSZ are relatively consistent within individual samples, where 2σ error is ≤ 7ppm with the exception of CB13-55a (430 m, discussed below). However, it is important to note that the detection limit on the EPMA is 11 ppm. Considering the instrumental detection limit along with the 2σ error on Ti concentrations, TitaniQ temperatures for all samples can be inferred to overlap within error. Furthermore, the assumption of a constant Ti activity across ~300 m of the shear zone width is likely oversimplified. We do not place much weight on the apparent variation of ~50 °C in TitaniQ temperatures from structurally high (446 m) to structurally low (134 m) positions. ASIM temperatures vary between samples beyond the error of the thermometer (50 °C). However, when considering error on the thermometer compounded with 2σ error on feldspar compositions, all ASIM temperatures also overlap.

Analysis on sample CB13-55a was conducted using a preliminary setup with three spectrometers (2 PET and 1 LLIF) with peak count times of 300 s on all three spectrometers or peak times of 300 s on PET and 600 s on LLIF spectrometers, yielding a detection limit between 13-22 ppm for individual analyses. Column conditions were 15 keV, 100 nA current, with a 20 µm beam size. Although this setup yields a less desirable detection limit and in turn introduces a greater uncertainty in Ti concentrations, the

average temperature, assuming α_{TiO_2} between 0.5 and 0.8, is within error of the ASIM-derived temperature, which is relatively well constrained with analysis of 14 myrmekite lobes.

A discrepancy exists between microstructurally vs. quantitatively derived temperatures for the deepest sample, CB13-54a (446 m). This sample preserves chessboard extinction within fractured feldspar (i.e. Fig. 5L) as well as grain boundary migration. Chessboard (CB) extinction is commonly attributed to basal <a> and prism [c] slip associated with the α-β transition in quartz (Kruhl, 1996). Even at the low pressures expected for the CBSZ (1-3 kb; Margirier et al., 2016), temperatures required for chessboard extinction are at least ~ 630 °C (Kruhl, 1996). Ti concentration is consistent between GBM and CB domains. This could be explained by an initially low Ti activity (~0.1) when CB occurred and increased Ti activity during deformation, by decreased Ti concentrations due to volume diffusion at high temperatures, by 'resetting' the Ti concentration at lower GBM temperatures, or simply by instrumental accuracy.

One sample that contained both GBM and SGR quartz recrystallization microstructures was analyzed for TitaniQ thermometry (CB13-79; 134 m). Ti-concentration (8 ± 6 ppm) was below the detection limit (11 ppm) of the electron probe microanalyzer (EPMA) at the University of Tennessee. SGR microstructures could indicate higher-strain rather than lower temperature conditions than those occurring during GBM recrystallizaiton, such that the Ti concentration would still be consistent with concentrations expected at relatively high temperatures. However, our analysis of this sample suggests that TitaniQ analysis especially for samples with SGR recrystallization microstructures is not viable without more precise instrumentation.

REFERENCES

Cross, A.J., Kidder, S.B., and Prior, D.J., 2015, Using microstructures and TitaniQ thermobarometry of quartz sheared around garnet porphyroclasts to evaluate microstructural evolution and constrain an Alpine Fault Zone geotherm: Journal of Structural Geology, v. 75, p. 17–31, doi: 10.1016/j.jsg.2015.02.012.

Götze, J., 2002, Potential of cathodoluminescence (cl) microscopy and spectroscopy for the analysis of minerals and materials: Analytical and Bioanalytical Chemistry, v. 374, p. 703–708, doi: 10.1007/s00216-002-1461-1.

Haertel, M., Herwegh, M., and Pettke, T., 2013, Titanium-in-quartz thermometry on synkinematic quartz veins in a retrograde crustal-scale normal fault zone: Tectonophysics, v. 608, p. 468–481, doi: 10.1016/j.tecto.2013.08.042.

Hielscher, R., and Schaeben, H., 2008, A novel pole figure inversion method: Specification of the MTEX algorithm: Journal of Applied Crystallography, v. 41, p. 1024–1037, doi: 10.1107/S0021889808030112.

Huang, R., and Audétat, A., 2012, The titanium-in-quartz (TitaniQ) thermobarometer: A critical examination and re-calibration: Geochimica et Cosmochimica Acta, v. 84, p. 75–89, doi: 10.1016/j.gca.2012.01.009.

Kruhl, J.H., 1996, Prism- and basal-plane parallel subgrain boundaries in quartz: a microstructural geothermobaromether: Journal of Metamorphic Geology, v. 14, p. 581–589, doi: 10.1046/j.1525-1314.1996.00413.x.

Mainprice, D.H., Bachmann, F., Hielscher, R., and Schaeben, H., 2015, Descriptive tools for the analysis of texture projects with large datasets using MTEX: strength, symmetry and components: Geological Society, London, Special Publications, v. 409, doi: 10.1144/SP409.8.

Margirier, A., Audin, L., Robert, X., Herman, F., Ganne, J., and Schwartz, S., 2016, Time and mode of exhumation of the Cordillera Blanca batholith (Peruvian Andes): Journal of Geophysical Research: Solid Earth, v. 121, p. 6235–6249, doi: 10.1002/2016JB013055.

Nachlas, W.O., and Hirth, G., 2015, Experimental constraints on the role of dynamic recrystallization on resetting the Ti-in-quartz thermobarometer: Journal of Geophysical Research: Solid Earth, v. 120, p. 8120–8137, doi: 10.1002/2013JB010742.Changes.

Thomas, J.B., Watson, E.B., Spear, F.S., Wark, D.A., Thomas, J.B., Watson, E.B., and Spear, F.S., 2015, TitaniQ recrystallized: experimental confirmation of the original Ti-in-quartz calibrations: Contrib Mineral Petrol, v. 169, doi: 10.1007/s00410-015-1120-0.

Xia, H., and Platt, J.P., 2018, Is the Vincent fault in southern California the Laramide subduction zone megathrust ? , p. 1–17, doi: 10.1130/B31870.1/4301894/b31870.pdf.
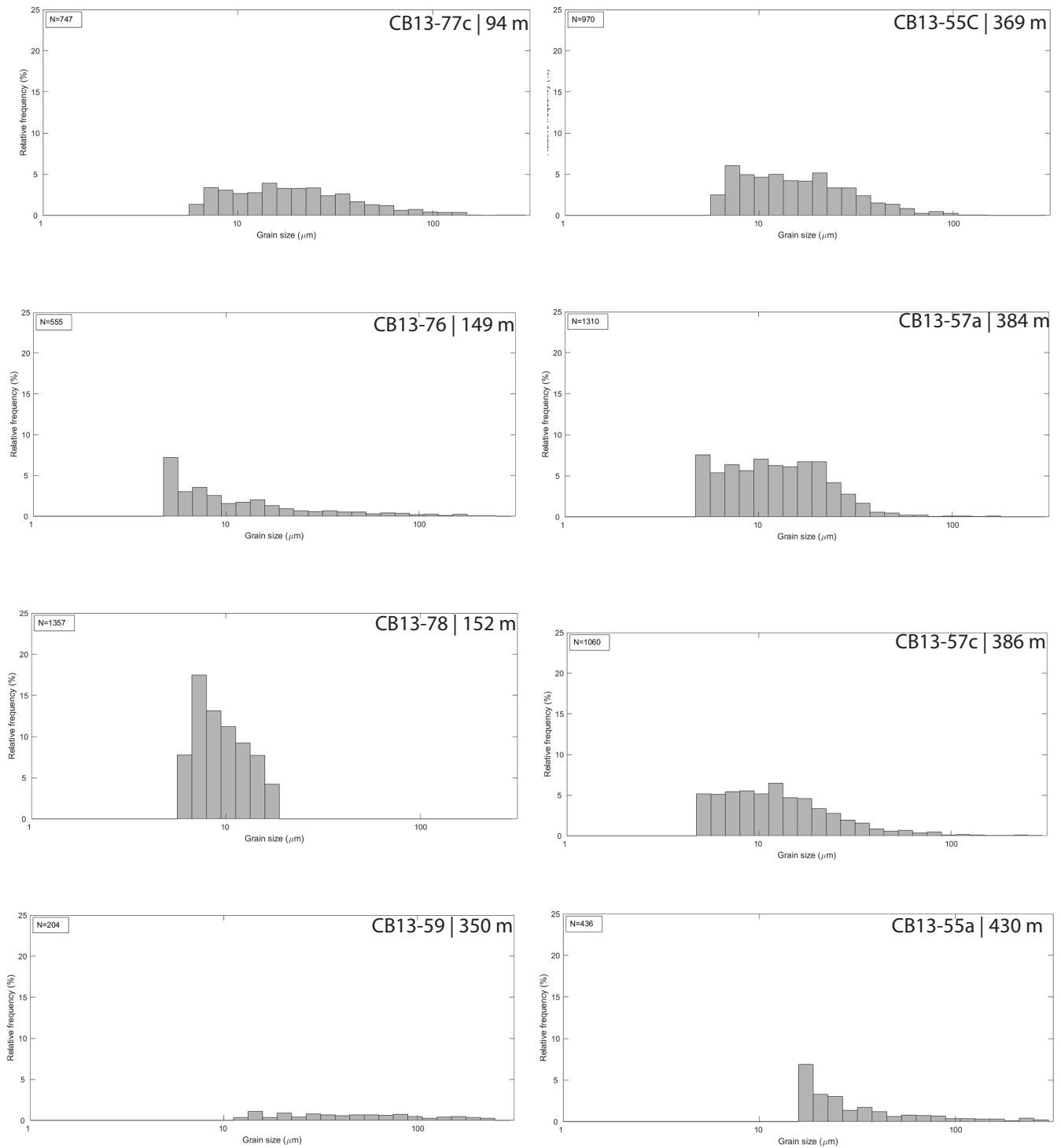
Supplementary figure S1. Quartz recrystallized grain size distributions. Number of grains in each population (N) in upper left corner. Sample numbers listed with structrual depth below the detachment.
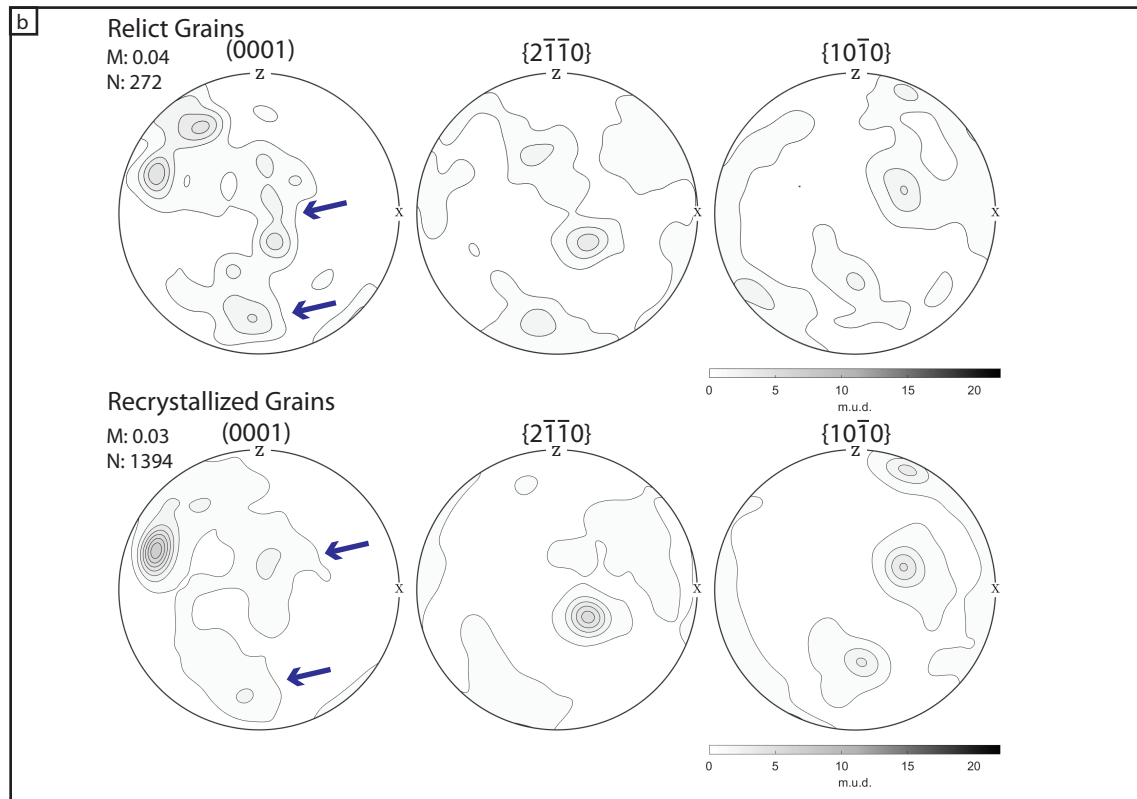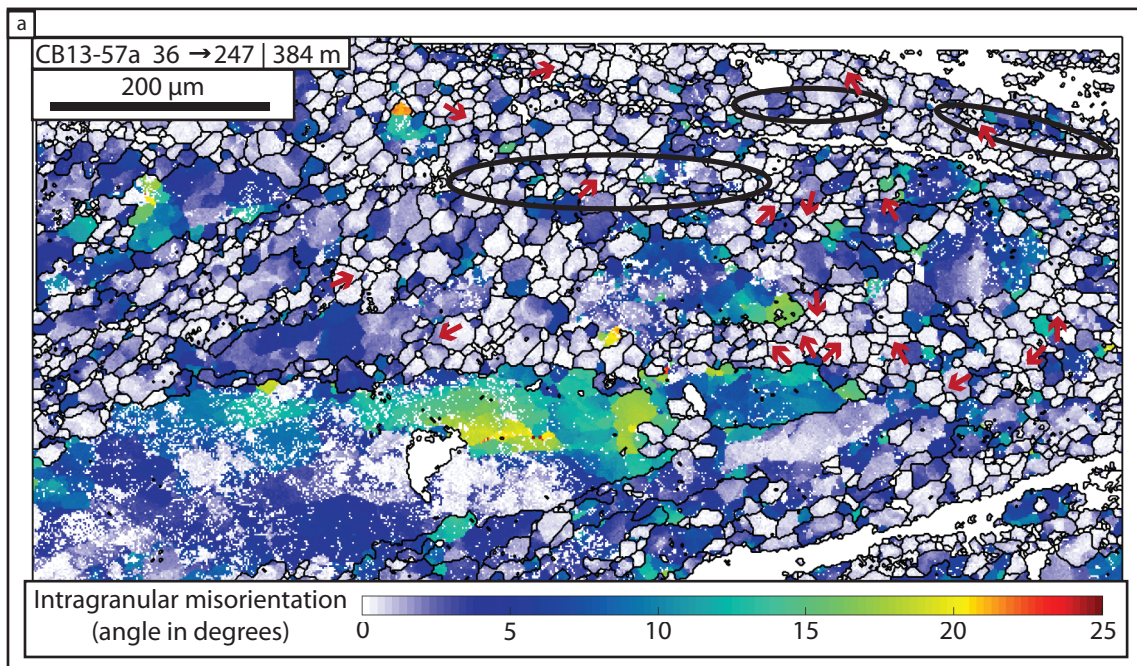
Supplementary figure S2. EBSD-based evidence for grain boundary sliding in CB13-57a (384 m). a) map of intragranular misorientations (relative to mean orientation of grain) using 'mis2mean' property in MTEX toolbox for MATLAB. Grain boundaries shown in black, critical misorientation: 10 degrees. Thick black ellipses highlight aligned grain boundaries. Red arrows point to 4-grain junctions. b) 1 point per grain pole figures of crystallographic preferred orientations for relict quartz grains (upper) and recrystallized quartz grains (lower). Note the dispersion of weak maxima near the central (Y-direction) and lower perihphal areas in the recyrstallized pole figure relative to the relict pole figure (blue arrows).